Istraživanja i projektovanja za privredu
ISSN 1451-4117
DOI:10.5937/jaes0-50225
www.engineeringscience.rs

iipp publishing

Journal of Applied Engineering Science
Vol. 22, No. 2, 2024
Original Scientific Paper
Paper number: 22(2024)2, 1213, 492-505

PROCESS MONITORING IN HYBRID ELECTRIC VEHICLES BASED ON DYNAMIC NONLINEAR METHOD

Yonghui Wang[1,2], Syamsunur Deprizon[1,3]*, Chun Kit Ang [4], Peng Cong[1], Zhiming Zhang[4]

[1] Faculty of Engineering, Technology and Built Environment, UCSI University, Kuala Lumpur, Malaysia
[2] College of Urban Transportation and Logistics, Shenzhen Technology University, Shenzhen, China
[3] Postgraduate Department, Universitas Bina Darma Palembang, Indonesia
[4] Faculty of Engineering, UCSI University, Taman Connaught, Kuala Lumpur, Malaysia
** deprizon@ucsiuniversity.edu.my*

Highway third-level faults can significantly deteriorate the reliability and performance of hybrid electric vehicle (HEV) powertrains. This study presents a novel process monitoring method aimed at addressing this issue. We propose a multivariate statistical method based on dynamic nonlinear improvement, namely dynamic neural component analysis (DNCA). This method does not require the establishment of precise analytical models; instead, it only necessitates acquiring data from HEV powertrains. Through numerical simulation and real HEV experiments, we demonstrate the effectiveness of this approach in monitoring highway third-level faults. The testing outcomes demonstrate that DNCA outperforms traditional dynamic methods like dynamic principal component analysis (DPCA), conventional nonlinear methods such as kernel PCA (KPCA) and NCA, as well as traditional dynamic nonlinear methods like DKPCA.

Keywords: dynamic neural component analysis, dynamic nonlinear improvement, highway third-level faults, hybrid electric vehicle, multivariate statistical method, process monitoring

1 INTRODUCTION

Process monitoring, widely implemented in hybrid electric vehicles (HEVs), plays a crucial role in guaranteeing the optimal performance, reliability, and safety of HEV powertrain [1-3]. It allows for timely intervention, maintenance, or corrective actions to prevent potential faults, optimize energy efficiency, and prolong the lifespan of critical components. As the number of HEVs increases, the occurrences of highway faults involving HEVs are also on the rise. These faults can have significant impacts on HEVs, including loss of power, reduced efficiency, safety risks, and increased maintenance costs. The classifications of highway faults categorize the severity of vehicle malfunctions, typically guiding both troubleshooting and emergency responses. Here are the common classifications:

- Highway first-level faults: Highway first-level faults refer to issues that affect HEV performance but do not immediately endanger safety. For instance, minor mechanical or electronic system faults may result in partial loss of functionality, yet the HEV can still be safely driven to the nearest service point for repair.
- Highway second-level faults: Highway second-level faults involve problems that affect HEV safety performance but do not immediately pose a danger. This may include brake system faults, tire punctures, or electrical system faults. Drivers may need to take some measures such as reducing speed or replacing a spare tire to ensure safety.
- Highway third-level faults: Highway third-level faults denote issues that significantly compromise HEV safety, potentially leading to accidents or rendering the HEV inoperable. Examples include engine faults, steering system faults s, or severe brake faults. In the event of highway third-level faults, drivers need to take immediate emergency measures such as quickly moving the HEV to a safe area and seeking professional assistance.

Highway third-level faults in HEV powertrains can result in sudden loss of power, rendering the HEV unable to continue driving. Such occurrences may stem from engine, transmission, or electric motor faults, significantly compromising the HEV's reliability and performance. However, compared to traditional internal combustion engine vehicles, the variables within HEV powertrain exhibit interactions and complex dynamic relationships. The variations in these variables are influenced not only by driving modes, road conditions, and environmental factors but also by the structure of the powertrain system itself and its control strategies [4-6]. Therefore, the operating state of HEV powertrain systems often demonstrates characteristics of nonlinearity and dynamic changes, which increase the difficulty of process monitoring.

Process monitoring methods can generally be categorized into three types: those based on empirical knowledge, analytical models, and data-driven approaches [7-9]. Empirical knowledge-based process monitoring methods rely on the expertise and experience of individuals or groups to develop monitoring strategies [10, 11]. These methods typically involve the use of qualitative information, rules, or heuristics derived from prior knowledge or observations of the system's behavior. They can be classified into three main categories: qualitative simulation methods [12, 13], graph theory methods [14, 15], and expert system methods [16, 17]. However, these methods may struggle to adapt to changing system conditions or environments, as they rely on static rules or heuristics derived from past experience.

Additionally, they may lack the ability to handle complex systems with nonlinear dynamics or large amounts of data, limiting their effectiveness in HEV powertrain applications. Analytical models rely on mathematical models to represent the underlying processes and relationships within a system [18, 19]. These methods can be classified into three main categories: state estimation methods [20, 21], parameter estimation methods [22, 23], and equivalence space methods [24]. However, the powertrain systems of HEVs have become increasingly complex due to advancements in technology and the integration of various components such as internal combustion engines, electric motors, and sophisticated control systems. In light of this complexity, traditional process monitoring methods based on analytical models are no longer adequate because they may be limited by the availability of accurate models, computational complexity, and sensitivity to measurement noise or errors in the data. Data-driven methods have emerged as powerful tools for process monitoring and analysis in various domains, including HEV powertrain systems [25-27]. These methods leverage the abundance of data generated by sensors and onboard systems to capture complex relationships and patterns within the system. Multivariate statistics process monitoring (MSPM) methods, as the most widely used data-driven approaches, utilize statistical techniques to study the relationships and interactions between variables, as well as their impact on the overall structure of the data. Figure 1 shows the flowchart of MSPM methods.

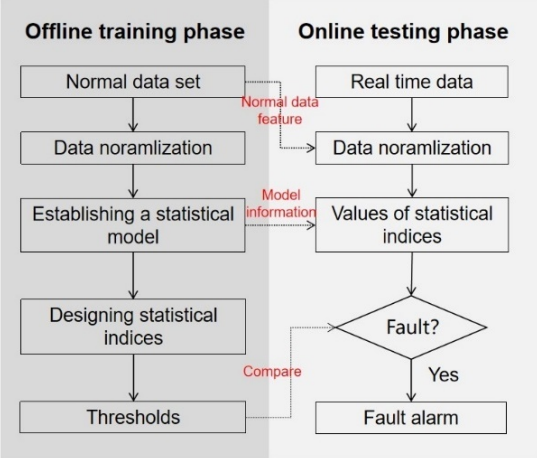

Fig. 1. Flowchart of MSPM methods [28]

The most frequently utilized nonlinear method for addressing nonlinear process monitoring challenges is kernel principal component analysis (KPCA) [29-31]. While KPCA employs kernel functions to delineate nonlinear data relationships, it necessitates the definition of parameters initially. Consequently, this approach lacks prior parameter tuning knowledge and does not update parameters during the training phase. However, the consideration of autocorrelation among variables also plays a crucial role in ensuring the reliability and accuracy of monitoring systems. To address the dynamic process monitoring issues, Negiz et al. [32] proposed a method based on time series models in 1994, but this approach is only suitable for monitoring data without correlation between variables. Ku et al. [33] introduced dynamic PCA (DPCA) for capturing the dynamic characteristics of process data using delayed extension matrices in 1995, aiming to mitigate the impact of data dynamics on process monitoring. The effectiveness of this method has been validated by a series of studies and has been widely applied. To address both dynamic and nonlinear issues simultaneously, Choi et al. [34] introduced the dynamic KPCA (DKPCA) approach in 2004, amalgamating DPCA and KPCA to realize dynamic nonlinear process monitoring. Typically, the parameters for both KPCA and DKPCA require adjustment through trial and error, rendering them suboptimal for nonlinear processes, thus constraining their effectiveness [35]. To improve the nonlinear ability of PCA, Lou and Wang [36] proposed neural component analysis (NCA), which is the combination of artificial neural network (ANN) and PCA.

Drawing inspiration from DPCA and NCA, this paper introduces a novel approach termed dynamic NCA (DNCA) aimed at tackling dynamic and nonlinear challenges in process monitoring. The contributions of this study can be outlined as follows: Firstly, due to the dynamic characteristics in the highway third-level fault data, this paper employs the time lag shift method to construct an augmented matrix of the data prior to applying the NCA method for monitoring nonlinear relationships within the dataset. Secondly, in order to enhance capability of monitoring the dynamic relationships of highway third-level faults in HEV, this paper proposes a method for determining the order of the time lag shift model and compares it with the Bayesian information criterion (BIC) method. Finally, this paper employs a dynamic nonlinear model to validate the dynamic nonlinear monitoring capability of the proposed method, and applies it to actual HEV highway third-level fault data. The testing outcomes demonstrate that DNCA outperforms traditional dynamic methods like DPCA, conventional nonlinear methods such as KPCA and NCA, as well as traditional dynamic nonlinear methods like DKPCA.

The structure of this paper is organized into five sections: Section 2 elaborates on the proposed DNCA method. Section 3 establishes a dynamic nonlinear model to compare the efficacy of DNCA, DPCA, KPCA, NCA, and DKPCA. Section 4 compares the performance of the traditional four methods and the proposed DNCA method in Kinglong HEV powertrain systems. Finally, Section 5 summarizes the key findings and conclusions drawn from this study.

2 METHODS

2.1 Time Lag Shift Method

For PCA offline learning, a set of n training samples is provided, with the s original process variables denoted as $\boldsymbol{X} \in \boldsymbol{R}^{n\times s}$. PCA divides $\boldsymbol{X}$ into the following subspaces:

$$\boldsymbol{X} = \boldsymbol{T}\boldsymbol{P}^T + \boldsymbol{E}, \tag{1}$$

where $\boldsymbol{T} \in \boldsymbol{R}^{n\times k}$ represents the score matrix containing the main information; $\boldsymbol{P} \in \boldsymbol{R}^{s\times k}$ is the projection matrix from $\boldsymbol{X}$ to $\boldsymbol{T}$; $\boldsymbol{E} \in \boldsymbol{R}^{n\times s}$ denotes the residual subspaces that should not be monitored. k is the number of principal components (PCs), which can be determined by cumulative percent variance (CPV) as shown in Eq. (2).

$$CPV\% = \frac{\sum_{i=1}^{k}\lambda_i}{\sum_{i=1}^{s}\lambda_i} \times 100\% \geq 85\%. \tag{2}$$

where $\lambda_i (i = 1,2,...,k,...,m)$ represents the i-th eigenvalue sorted in descending order. If CPV% is greater than the set threshold, which often equals to 85%, and the corresponding k should be set as the number of PCs.

Traditional PCA method overlooks temporal dynamics, failing to capture changes and dynamic characteristics in time-series data effectively. Therefore, the original process variables at the current time t can expanded by DPCA:

$$\tilde{\boldsymbol{X}}(t) = \left[\boldsymbol{X}(t), \boldsymbol{X}(t-1), ..., \boldsymbol{X}(t-q)\right] \in \boldsymbol{R}^{1\times[(q+1)\times s]}, \tag{3}$$

where $\tilde{\boldsymbol{X}} \in \boldsymbol{R}^{n\times[(q+1)\times s]}$ is the augmented matrix; q is the order of the DPCA model, which is the key parameter that determines the effectiveness of the time lag shift method. To provide a novel method for determining q, consider the association with the current and past time data as follows:

$$\boldsymbol{X}(t) = \boldsymbol{X}(t-1)\boldsymbol{A}_1 + \boldsymbol{X}(t-2)\boldsymbol{A}_2 + ... + \boldsymbol{X}(t-q)\boldsymbol{A}_q + \boldsymbol{B}(t), \tag{4}$$

where $\tilde{\boldsymbol{A}} = \left[\boldsymbol{A}_1, \boldsymbol{A}_2, ..., \boldsymbol{A}_q\right] \in \boldsymbol{R}^{n\times[q\times s]}$ denotes the coefficient matrix characterizing the relationship between variables at the current time and past times; $\boldsymbol{B}(t)$ denotes the disturbance introduced at each time step, and it is statistically independent of variables at previous time steps. In such a dynamic system, the goal is to minimize the noise introduced at each moment in time. Firstly, the coefficient matrix $\tilde{\boldsymbol{A}}$ can be estimated using the least square method as follows:

$$\tilde{\boldsymbol{A}} = \left[\tilde{\boldsymbol{X}}^T(t)\tilde{\boldsymbol{X}}(t)\right]^{-1}\tilde{\boldsymbol{X}}^T(t)\boldsymbol{X}(t). \tag{5}$$

Secondly, the disturbance $\boldsymbol{B}(t)$ can be estimated as follows:

$$\boldsymbol{B}(t) = \boldsymbol{X}(t) - \boldsymbol{X}(t)\tilde{\boldsymbol{A}} = \boldsymbol{X}(t) - \boldsymbol{X}(t)\left[\tilde{\boldsymbol{X}}^T(t)\tilde{\boldsymbol{X}}(t)\right]^{-1}\tilde{\boldsymbol{X}}^T(t)\boldsymbol{X}(t). \tag{6}$$

Finally, the optimal number of q can be determined if the index Q decreases gradually and no longer undergoes significant changes as q increases.

$$Q = \left\|\sum_{t=1}^{n}\boldsymbol{B}(t)\right\|^2 = \left\|\boldsymbol{X} - \tilde{\boldsymbol{X}}[\tilde{\boldsymbol{X}}^T\tilde{\boldsymbol{X}}]^{-1}\tilde{\boldsymbol{X}}^T\boldsymbol{X}\right\|^2. \tag{7}$$

2.2 Dynamic Neural Component Analysis

DPCA excels in extracting the uncorrelated PCs $\boldsymbol{I}_j$ $(j = 1,2,...,k)$ from autocorrelated variables, while NCA is proficient in nonlinear process monitoring. Inspired by the capabilities of DPCA and NCA, a three-layer DNCA network can be constructed, as illustrated in Fig. 2.

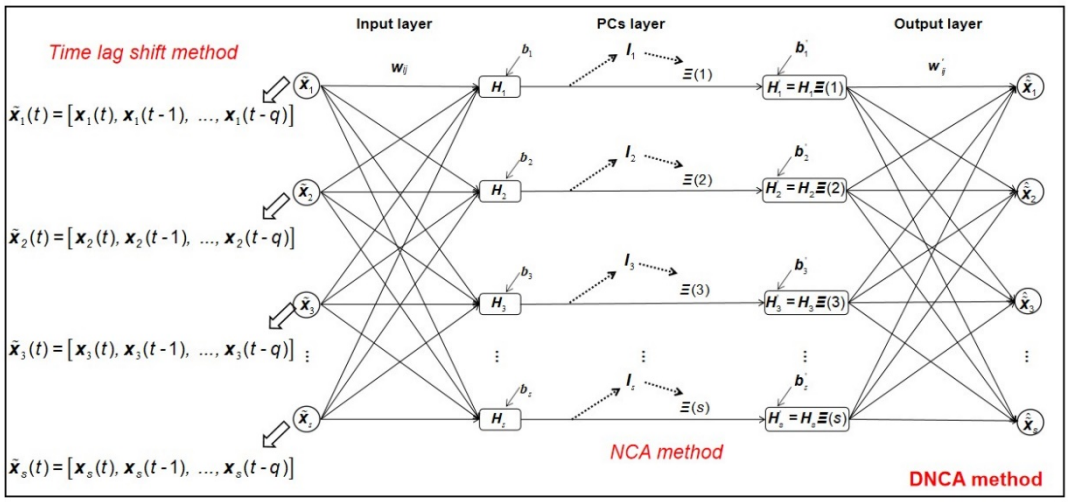

Fig. 2. Principle of the DNCA method

The DNCA network is constructed based on the following DPCA criteria:

– **Criteria 1:** all PCs extracted from autocorrelated variables are uncorrelated.

To satisfy this criterion, components $\boldsymbol{I}_j$ $(j=1,2,...,s)$ must be uncorrelated, implying that the correlation coefficient $r_{i,j}=\dfrac{cov(\boldsymbol{I}_i,\boldsymbol{I}_j)}{\sqrt{D(\boldsymbol{I}_i)}\sqrt{D(\boldsymbol{I}_j)}}=0\,(i\neq j)$, where $cov(\cdot)$ represents the covariance function and $D(\cdot)$ represents the variance function. Consequently, the cost function E_1 is formulated for DNCA:

$$E_1=\frac{1}{s(s-1)}\sum_{m=1}^{s}\sum_{l=1,l\neq m}^{s}\left(\frac{cov(\boldsymbol{I}_m,\boldsymbol{I}_l)}{\sqrt{D(\boldsymbol{I}_m)}\sqrt{D(\boldsymbol{I}_l)}}\right)^2=\frac{1}{s(s-1)}\sum_{m=1}^{s}\sum_{l=1,l\neq m}^{s}\frac{(cov(\boldsymbol{I}_m,\boldsymbol{I}_l))^2}{D(\boldsymbol{I}_m)D(\boldsymbol{I}_l)}$$

$$=\frac{1}{s(s-1)}\sum_{m=1}^{s}\sum_{l=1,l\neq m}^{s}\frac{\left(\frac{1}{n}\sum_{t=1}^{n}\boldsymbol{I}_m(t)\boldsymbol{I}_l(t)-\frac{1}{n^2}\sum_{t=1}^{n}\boldsymbol{I}_m(t)\sum_{t=1}^{n}\boldsymbol{I}_l(t)\right)^2}{\left(\frac{1}{n}\sum_{t=1}^{n}\boldsymbol{I}_m(t)\boldsymbol{I}_m(t)-\frac{1}{n^2}\sum_{t=1}^{n}\boldsymbol{I}_m(t)\sum_{t=1}^{n}\boldsymbol{I}_m(t)\right)\left(\frac{1}{n}\sum_{t=1}^{n}\boldsymbol{I}_l(t)\boldsymbol{I}_l(t)-\frac{1}{n^2}\sum_{t=1}^{n}\boldsymbol{I}_l(t)\sum_{t=1}^{n}\boldsymbol{I}_l(t)\right)} \tag{8}$$

– **Criteria 2:** only a few components with the largest variances are selected as PCs.

To fulfill this criterion, the PCs picker score $\boldsymbol{\Xi}(j)$ (j=1, 2, …, s) is determined through the following steps:

Step 1: calculate the variance of each component.

Step 2: sort them in descending order and denote them as $\{\lambda_i\}$. Then determine the number of PCs k according to Eq. (2). Finally, set $\text{var}_{\text{stand}}=\dfrac{\lambda_k+\lambda_{k+1}}{2}$;

Step 3: compute $\boldsymbol{\Xi}(j)=\dfrac{\text{sign}(\text{D}(\boldsymbol{I}_j)-\text{var}_{\text{stand}})+1}{2}$ for each component. If $\boldsymbol{\Xi}(j)=1$, the component $\boldsymbol{I}_j$ is picked as the PC.

– **Criteria 3:** reconstruction error between the outputs and inputs should be minimized.

To fulfill this criterion, the cost function E_2 is formulated for DNCA:

$$E_2=\frac{1}{sn}\sum_{t=1}^{n}\sum_{m=1}^{s}(\boldsymbol{x}_m(t)-\hat{\boldsymbol{x}}_m(t))^2 \tag{9}$$

– **Criteria 4:** if all components are selected as PCs ($\boldsymbol{\Xi}(j)=1$) in DPCA, the outputs should be equal to the inputs.

To fulfill this criterion, set $\boldsymbol{b}_j'=-\boldsymbol{b}_j$ and $\boldsymbol{w}'=\boldsymbol{w}^{-1}$. When all $\boldsymbol{\Xi}(j)=1$, one gets:

$$\hat{\boldsymbol{X}}^T=\boldsymbol{w}'(\boldsymbol{H}'+\boldsymbol{b}')=\boldsymbol{w}^{-1}(\boldsymbol{H}-\boldsymbol{b})=\boldsymbol{w}^{-1}\boldsymbol{w}\boldsymbol{X}^T=\boldsymbol{X}^T. \tag{10}$$

To avoid the convergence problem, E_1 and E_2 are integrated into one:

$$E=\sigma E_1+E_2, \tag{11}$$

where σ is a parameter for balancing E_1 and E_2. Utilizing the gradient descent method, we have:

$$\begin{cases} \dfrac{\partial E}{\partial \boldsymbol{w}_{ij}} = \sigma \dfrac{\partial E_1}{\partial \boldsymbol{w}_{ij}} + \dfrac{\partial E_2}{\partial \boldsymbol{w}_{ij}} \\ \dfrac{\partial E}{\partial \boldsymbol{b}_j} = \sigma \dfrac{\partial E_1}{\partial \boldsymbol{b}_j} + \dfrac{\partial E_2}{\partial \boldsymbol{b}_j} \end{cases}. \tag{12}$$

The adjustment of parameters $\{\boldsymbol{w}_{ij}\}$ and $\{\boldsymbol{b}_j\}$ should be proportional to the gradient of the error:

$$\begin{cases} \boldsymbol{w}_{ij}^{ite+1} = \boldsymbol{w}_{ij}^{ite} - \alpha \dfrac{\partial E}{\partial \boldsymbol{w}_{ij}^{ite}} \\ \boldsymbol{b}_j^{ite+1} = \boldsymbol{b}_j^{ite} - \alpha \dfrac{\partial E}{\partial \boldsymbol{b}_j^{ite}} \end{cases}, \tag{13}$$

where *ite* is the iteration number, and α is the learning rate.

3 NUMERICAL EXAMPLES

3.1 Dynamic nonlinear numerical model

A dynamic nonlinear model was utilized to evaluate and compare the performance of DNCA, DPCA, KPCA, NCA, and DKPCA. The simulated process was described by Eq. (14):

$$\boldsymbol{x}(t) = \begin{bmatrix} 2\boldsymbol{x}(t-1)sin(\boldsymbol{x}(t-1)) \\ 5cos(\boldsymbol{x}(t-2)) \end{bmatrix}^T \boldsymbol{C} + \begin{bmatrix} 10e^{\boldsymbol{N}_1(t)} + 20 \\ 10\boldsymbol{N}_2^2(t) + \boldsymbol{N}_2(t) \end{bmatrix}^T \boldsymbol{D} + 0.01\boldsymbol{\omega}(t), \tag{14}$$

where $\boldsymbol{N}_1$ and $\boldsymbol{N}_2$ are independent variables following standard Gaussian distributions, and $\boldsymbol{\omega}(t) = [\boldsymbol{\omega}_1(t), \boldsymbol{\omega}_2(t), ..., \boldsymbol{\omega}_5(t)]^T$ represents the noise introduced at each time. $\boldsymbol{C}$ is the dynamic coefficient matrix, and $\boldsymbol{D}$ is the nonlinear static coefficient matrix. They are defined as follows:

$$\boldsymbol{C} = \begin{bmatrix} 0.30 & -0.15 & 0.45 & 0.00 & 0.00 & 0.30 & -0.15 & -0.45 & 0.00 & 0.00 \\ 0.00 & -0.30 & 0.60 & 0.60 & 0.15 & 0.00 & -0.30 & -0.60 & 0.60 & -0.45 \\ 0.00 & 0.75 & 0.00 & 0.00 & -0.45 & 0.00 & 0.75 & 0.75 & 0.00 & -0.45 \\ -0.30 & 0.00 & 0.45 & 0.00 & 0.30 & -0.30 & 0.00 & 0.45 & 0.00 & 0.30 \\ -0.15 & 0.00 & 0.75 & 0.15 & -0.30 & -0.15 & 0.00 & 0.75 & 0.15 & -0.30 \end{bmatrix}^T \tag{15}$$

$$\boldsymbol{D} = \begin{bmatrix} 1 & 1 & 2 & 2 & 2 \\ 2 & 0 & 1 & 0 & 2 \end{bmatrix} \tag{16}$$

Offline modeling involved approximately 500 normal samples. Time lag shift method typically employs the BIC criterion to determine the value of parameter *q*. The parameter *q* calculated using the BIC criterion in this study is 4, as shown in Figure 3. However, the variables at the current time are correlated with the variables from the past two-time steps, indicating that the value of *q* should be 2. The reason for this is that the BIC criterion is based on a linear approximation of the logarithm of the likelihood function, hence it may not be applicable in the case of nonlinear models.

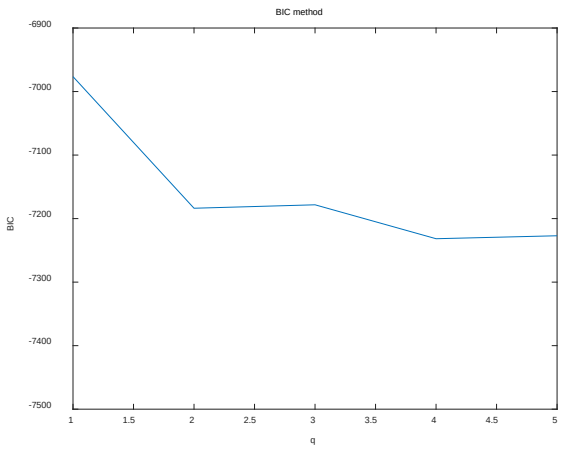

Fig. 3. Values of index *Q* calculated using the BIC method under different *q* values

To determine the correct value of parameter q, calculate the value of index Q under different q values, as shown in Figure 4. The optimal number of q can be determined if the index Q decreases gradually and no longer undergoes significant changes as q increases.

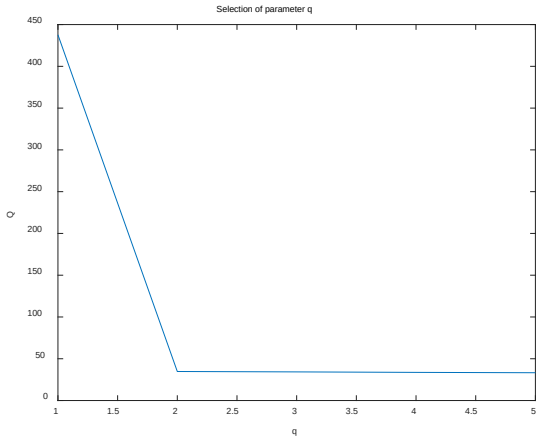

Fig. 4. Values of index Q calculated using the proposed method under different q values.

From the above figure, it can be observed that the value of index Q reaches a local minimum at q=2. As the value of q is further increased, Q continues to increase without significant changes. Therefore, the method described in this paper correctly determines the value of q. This method is intuitive and simple. Unlike BIC, it does not require complex statistical assumptions about the model structure. It can adapt to various types of time series.

3.2 Comparative experiment

Online testing generated 50 normal samples and 450 fault samples, which were subsequently monitored using the I^2 and SPE indices, as depicted below.

$$I^2(t') = \frac{1}{s(s-1)} \sum_{m=1}^{s} \sum_{l=1, l\neq m}^{s} r_{\mathrm{m,l}}^2 (t'-T+1, t)$$

$$= \frac{1}{s(s-1)} \sum_{m=1}^{s} \sum_{l=1, l\neq m}^{s} \frac{\left(\frac{1}{T} \sum_{t=t'-T+1}^{t'} \boldsymbol{I}_{\mathrm{m}}(t) \boldsymbol{I}_{\mathrm{l}}(t) - \frac{1}{T^2} \sum_{t=t'-T+1}^{t'} \boldsymbol{I}_{\mathrm{m}}(t) \sum_{t=t'-T+1}^{t'} \boldsymbol{I}_{\mathrm{l}}(t) \right)^2}{\left(\frac{1}{T} \sum_{t=t'-T+1}^{t'} \boldsymbol{I}_{\mathrm{m}}(t)^2 - \frac{1}{T^2} \left(\sum_{t=t'-T+1}^{t'} \boldsymbol{I}_{\mathrm{m}}(t) \right)^2 \right) \left(\frac{1}{T} \sum_{t=t'-T+1}^{t'} \boldsymbol{I}_{\mathrm{l}}(t)^2 - \frac{1}{T^2} \left(\sum_{t=t'-T+1}^{t'} \boldsymbol{I}_{\mathrm{l}}(t) \right)^2 \right)} \quad (17)$$

Since $r_{i,j}$ cannot be computed with one sample, it is necessary to consider the latest T samples to compute I^2 index and its threshold can be obtained through kernel density estimation (KDE). The SPE index for DNCA is constructed in the same manner as DPCA, and its threshold SPE_{lim} can also be obtained through KDE. If $SPE(t)$ exceeds its threshold, the subsequent two samples will be checked. And then if $SPE(t+1) > SPE_{\mathrm{lim}}$ and $SPE(t+2) > SPE_{\mathrm{lim}}$, a fault will be reported; otherwise, $SPE(t) = SPE(t-1)$.

The descriptions of the three faults are as follows:

Fault 1: an element in nonlinear static coefficient matrix ***D*** changed from 2 to -4. The fault detection rates (FDRs) and false alarm rates (FARs) for monitoring Fault 1 using five different methods are shown in Table 1. Data with excellent performance is highlighted in bold.

Table 1. FDRs and FARs for monitoring Fault 1

	Indices	dynamic method	nonlinear methods		dynamic nonlinear methods	
		DPCA	KPCA	NCA	DKPCA	DNCA
FARs	T^2 / I^2	0.00%	2.00%	0.00%	0.00%	0.00%
	SPE	0.00%	0.00%	0.00%	0.00%	0.00%
FDRs	T^2 / I^2	1.11%	65.04%	57.73%	24.12%	82.08%
	SPE	2.00%	64.82%	19.47%	49.12%	77.43%

From the results shown in Table 1, FARs of DPCA, NCA, DKPCA and DNCA exhibited excellent performance. However, DPCA was not sensitive to Fault 1 because it fails to consider the nonlinear problems. KPCA sacrificed its FAR performance in exchange for higher FDR, the FDR performance of KPCA even surpassed that of NCA. Although they were more sensitive than DPCA, they both failed to consider the autocorrelation problem and only identified 50%-60% fault samples. DKPCA, which simultaneously addresses autocorrelation and nonlinear issues, only identified 50% of fault samples due to insufficient nonlinear fitting capability. In contrast, DNCA performed best and its FDRs reached 70%-80%.

Fault 2: The autocorrelation matrix transforms into the following expression:

$$\begin{bmatrix} 2\boldsymbol{x}(t-1)sin(\boldsymbol{x}(t-1)) \\ 5cos(\boldsymbol{x}(t-2)) \end{bmatrix} \rightarrow \begin{bmatrix} 2\boldsymbol{x}(t-1)sin(\boldsymbol{-3x}(t-1)) \\ 5cos(\boldsymbol{x}(t-2)) \end{bmatrix}. \quad (18)$$

The FDRs and FARs for monitoring Fault 2 using five different methods are shown in Table 2. Data with excellent performance is highlighted in bold.

Table 2. FDRs and FARs for monitoring Fault 2

	Indices	dynamic method	nonlinear methods		dynamic nonlinear methods	
		DPCA	KPCA	NCA	DKPCA	DNCA
FARs	T^2 / I^2	0.00%	0.00%	0.00%	0.00%	0.00%
	SPE	0.00%	0.00%	0.00%	0.00%	0.00%
FDRs	T^2 / I^2	0.00%	0.00%	38.05%	10.40%	73.89%
	SPE	0.44%	0.00%	61.06%	10.62%	77.43%

Based on the findings presented in Table 2, the FARs of all methods demonstrated outstanding performance. However, DPCA and KPCA showed insensitivity to Fault 2. DPCA overlooks nonlinear issues, while KPCA neglects autocorrelation problems and lacks proficiency in capturing nonlinear features of variables. Even the combined DKPCA method, which integrates DPCA and KPCA, does not address the issue of poor nonlinear fitting capability. Therefore, its FDR values for T^2 and *SPE* indices were only around 10%. NCA exhibits stronger nonlinear fitting capability. Its FDR value for the I^2 index was approximately 40% higher than that of DPCA, KPCA, and DKPCA, while its FDR value for the *SPE* index was approximately 60% higher than that of them. However, it does not account for the autocorrelation of variables. Therefore, its FDR value for the I^2 index was approximately 35% lower than that of DNCA, and its FDR value for the *SPE* index was approximately 15% lower than that of DNCA.

Fault 3: element n_4 changed to n_4-1. The FDRs and FARs for monitoring Fault 3 using five different methods are shown in Table 3. Data with excellent performance is highlighted in bold.

Table 3. FDRs and FARs for monitoring Fault 1

	Indices	dynamic method	nonlinear methods		dynamic nonlinear methods	
		DPCA	KPCA	NCA	DKPCA	DNCA
FARs	T^2 / I^2	0.00%	0.00%	0.00%	0.00%	0.00%
	SPE	0.00%	0.00%	0.00%	0.00%	0.00%
FDRs	T^2 / I^2	0.00%	0.00%	57.74%	3.98%	95.35%
	SPE	0.00%	0.00%	0.00%	3.76%	95.13%

From the results shown in Table 3, FARs of DPCA, NCA, DKPCA and DNCA exhibited excellent performance. DPCA, KPCA, and DKPCA have inferior nonlinear fitting capabilities compared to NCA, resulting in their FDR values being approximately 50% lower than those of NCA. However, NCA does not account for the autocorrelation of variables. Therefore, its FDR value for the I^2 index was approximately 35% lower than that of DNCA, and its FDR value for the *SPE* index was approximately 95% lower than that of DNCA.

Below are the monitoring charts for Fault 1, with DPCA, KPCA, NCA, DKPCA, and DNCA as examples, highlighting the superiority of DNCA. Figure 5 illustrates the Fault 1 detection diagram of DPCA, where the blue line represents the index values and the red one represents the threshold values.

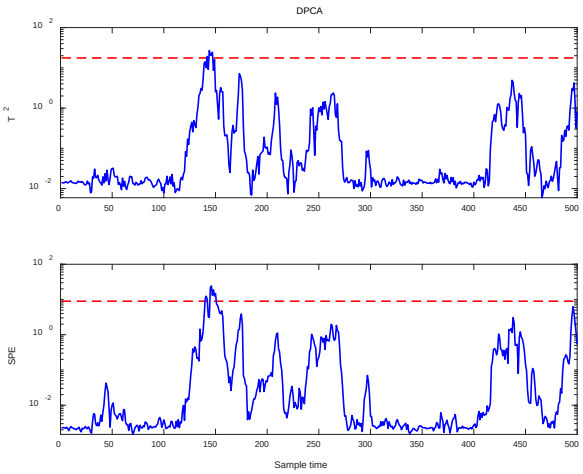

Fig. 5. Fault 1 detection diagram of DPCA

As shown in Figure 5, DPCA was not sensitive to Fault 1 and only identified it around the 150th sample. This is because DPCA only considers the autocorrelation of variables so that it is not good at capturing nonlinear feature of variables. Figure 6 illustrates the Fault 1 detection diagram of KPCA and NCA.

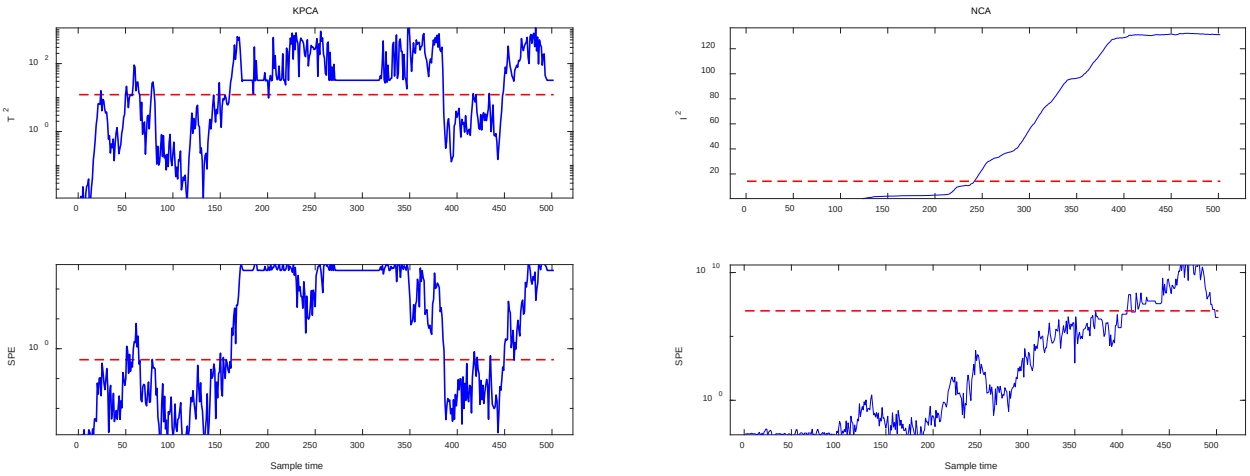

Fig. 6. Fault 1 detection diagram of KPCA and NCA

As illustrated in Figure 6, KPCA exhibits greater sensitivity to Fault 1 compared to NCA. This is evident from the fact that the T^2 index of KPCA detected Fault 1 at the 50th sample, while NCA identified it at the 242nd sample; the *SPE* index of KPCA detected Fault 1 at the 50th sample, while NCA identified it at the 406th sample. However, in both the early and late stages of Fault 1 occurrence, the values of indices in KPCA remained below the red line for a considerable duration. The reason for this occurrence is KPCA and NCA only consider the nonlinear feature of variables so that they are not good at capturing autocorrelation feature of them. Figure 7 shows the Fault 1 detection diagram of DKPCA and DNCA.

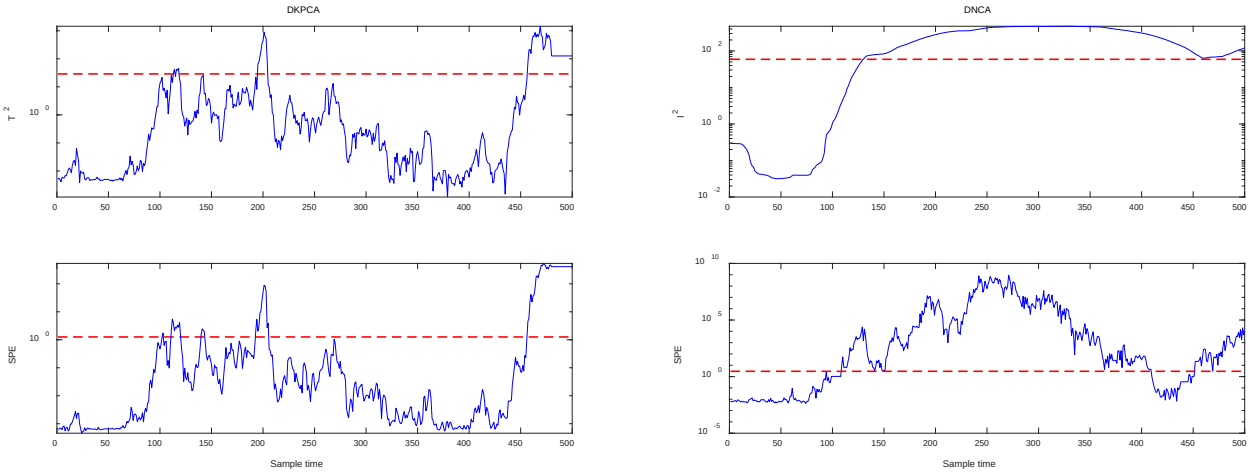

Fig. 7. Fault 1 detection diagram of DKPCA and DNCA

As illustrated in Figure 7, as a dynamic nonlinear method, DKPCA only surpassed the red line in indicator values around the 100th, 200th, and 450th samples, indicating its insensitivity to Fault 1. This is evident from the fact that DKPCA is not skilled at solving nonlinear problems. In contrast, from the 100th sample onwards, the values of DNCA's indices remained mostly above the red line, which indicates superior performance compared to all the aforementioned methods. To sum up, DNCA not only considers the autocorrelation issues but also possesses outstanding nonlinear fitting capability.

4 SIMULATION

4.1 Application object

Figure 8 indicates the considered powertrain system of Xiamen Kinglong HEV. This system seamlessly transitions between utilizing the internal combustion engine, the electric motor, or a combination of both to propel the vehicle, adapting flexibly to various driving modes.

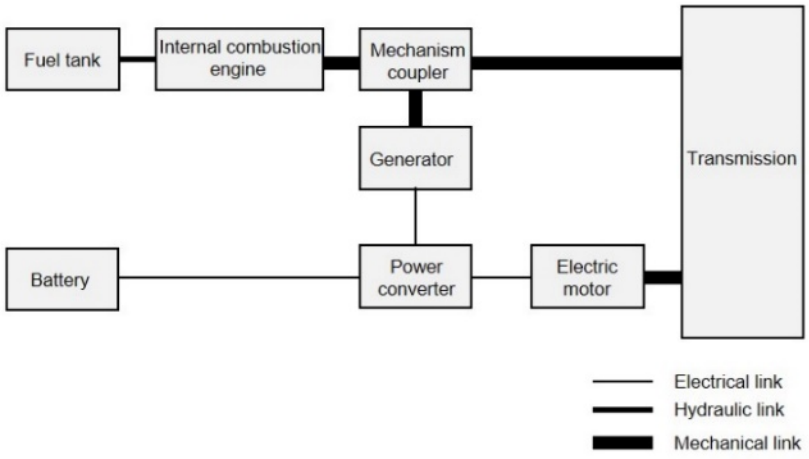

Fig. 8. Considered powertrain system of Xiamen Kinglong HEV

The technical specifications of Xiamen Kinglong HEV are shown in Table 4.

Table 4. Technical Specifications of Xiamen Kinglong HEV.

Motor parameters	
Peak power	135 *kW*
Rated power	85 *kW*
Maximum speed	3000 *r/min*
Rated speed	1700 *r/min*
Maximum torque	850 *Nm*
Rated torque	500 *Nm*
Engine parameters	
Rated power	147 *kW*
Rated torque	730 *Nm*

The method outlined in this paper has undergone testing at Xiamen Kinglong HEV. Several variables of the powertrain system are presented below:

Table 5. Definition of Variables

Variable number	Variable name	Variable number	Variable name
1	Actual torque of internal combustion engine (*Nm*)	10	Desired speed of electric motor (*r/s*)
2	Desired torque of internal combustion engine (*Nm*)	11	Temperature of electric motor (^oC)
3	Actual speed of internal combustion engine (*r/s*)	12	Current of electric motor (*A*)
4	Desired speed of internal combustion engine (*r/s*)	13	Accelerator pedal opening (*%*)
5	Water temperature (^oC)	14	Actual vehicle speed (*km/h*)
6	Oil temperature of internal combustion engine (^oC)	15	Desired vehicle speed (*km/h*)
7	Actual torque of electric motor (*Nm*)	16	Actual vehicle torque (*Nm*)
8	Desired torque of electric motor (*Nm*)	17	Desired vehicle torque (*Nm*)
9	Actual speed of electric motor (*r/s*)		

The experiment gathered data from highway third-level faults in HEV powertrain. The malfunction usually exhibits both nonlinear and autocorrelation characteristics simultaneously. Firstly, it is influenced by various complex factors that may have nonlinear relationships between variables. For example, interactions among factors such as engine load, vehicle speed, and temperature can lead to nonlinear effects. Secondly, during high-speed driving, the state of malfunction at one moment can influence the malfunction performance in subsequent moments, indicating autocorrelation characteristics in the time series. For instance, an engine overload at a specific moment may result in performance degradation for a period afterward, reflecting autocorrelation in the data.

4.2 Testing

The experiment collected data from 800 instances of the third-level malfunctions during high-speed driving. The training dataset comprises 500 instances of normal operating conditions, while the first 200 instances of the testing dataset represent normal operating conditions. Faults are introduced starting from the 201st sample. The parameter *q* chosen for DPCA, DKPCA and DNCA in this paper is 1. DPCA, KPCA, NCA, DKPCA and DNCA methods were used for comparison study, and their FARs and FDRs performance were shown in Table 6. Data with excellent performance is highlighted in bold.

Table 6. FARs and FDRs of five methods in HEV monitoring

	Indices	dynamic method	nonlinear methods		dynamic nonlinear methods	
		DPCA	KPCA	NCA	DKPCA	DNCA
FARs	T^2 / I^2	2.01%	0.00%	0.00%	0.00%	0.00%
	SPE	3.02%	100.00%	2.00%	1.51%	0.00%
FDRs	T^2 / I^2	80.00%	41.63%	89.75%	35.75%	95.35%
	SPE	73.38%	100.00%	81.63%	99.75%	95.13%

From the results shown in Table 6, only FARs of DNCA exhibited excellent performance and the *SPE* FAR of KPCA reached 100%, indicating its inability to differentiate between normal and fault data. As a dynamic method, the performance of DPCA is inferior to DKPCA and DNCA, which address non-linear problems. As a non-linear method, the performance of NCA is inferior to DKPCA and DNCA, which consider dynamic issues. The FDR performance of DKPCA's T^2 index is far inferior to that of DNCA's I^2 index, and its *SPE* FAR performance is also inferior to DNCA. Fig. 9 shows the HEV fault detection diagram of dynamic method---DPCA, where the blue line represents the index values and the red one represents the threshold values.

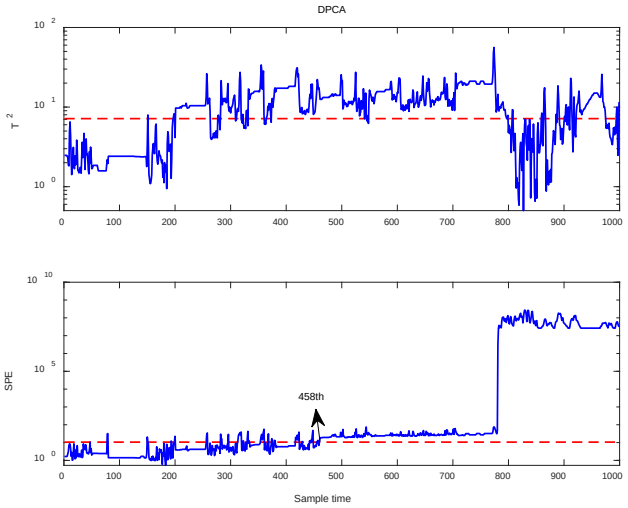

Fig. 9. HEV fault detection diagram of DPCA

From Fig. 9, it can be observed that in the case of DPCA, T^2 or *SP*E index exceeds the threshold even before faults occur. This could impact the time and cost for maintenance personnel. Additionally, the T^2 index value of DPCA fails to identify the occurrence of faults after the 800th sample, while its *SPE* index only detects faults effectively starting from the 458th sample. This may result in maintenance personnel being unable to promptly and effectively identify faults, thereby deteriorating the reliability and performance of HEV. This phenomenon occurs because the actual third-level highway fault data exhibit strong nonlinear characteristics, which DPCA does not consider in its monitoring. Fig. 10 illustrates the HEV fault detection using nonlinear methods—KPCA and NCA. In this figure, the blue line represents the index values, while the red line represents the threshold values.

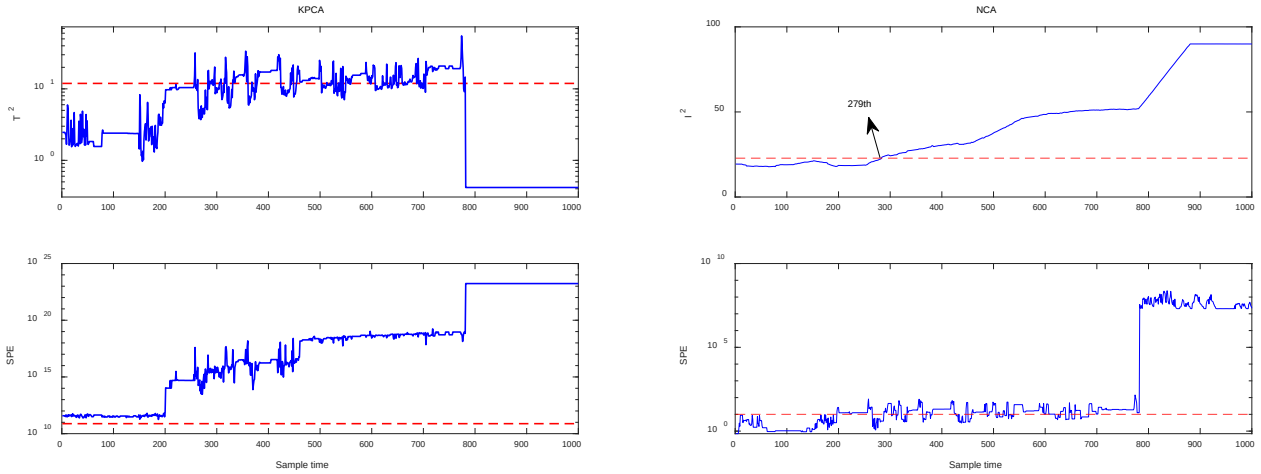

Fig. 10. HEV fault detection diagram of KPCA and NCA

From Fig. 10, it can be seen that in the case of KPCA, the values of the *SPE* index exceed the threshold before faults occur, indicating that it cannot distinguish between normal data and faults. Compared to KPCA, NCA has improved nonlinear fitting capability. This is evident from its performance in terms of FAR, which avoids the drawback of KPCA being unable to distinguish between normal data and faults entirely. Meanwhile, in KPCA, although most samples exceed the threshold for the T^2 index between the 200th and 800th samples, the value of the index starts to decrease significantly after the 800th sample. This may result in maintenance personnel being unable to promptly and effectively identify faults, thereby deteriorating the reliability and performance of HEV. This phenomenon occurs because KPCA does not consider the dynamic relationships between variables, and its nonlinear fitting capability is poor. On the other hand, NCA's I^2 index performs significantly better than KPCA, with most of the indices exceeding the threshold values. However, NCA only identifies the fault at the 279th sample, whereas the fault occurs at the 200th sample. Although NCA's *SPE* index detects the fault at the 200th sample, there are many samples between the 200th and 800th samples that do not exceed the threshold. This may lead maintenance personnel to mistakenly believe that the fault has been rectified, while the reliability and performance of the HEV will begin to deteriorate. The reason for this is that although NCA has strong nonlinear fitting capabilities, it does not consider the dynamic relationships between variables. Therefore, a method is needed to address NCA's dynamic monitoring issues. Fig. 11 shows the HEV fault detection diagram of dynamic nonlinear methods---DKPCA and DNCA, where the blue line represents the index values and the red one represents the threshold values.

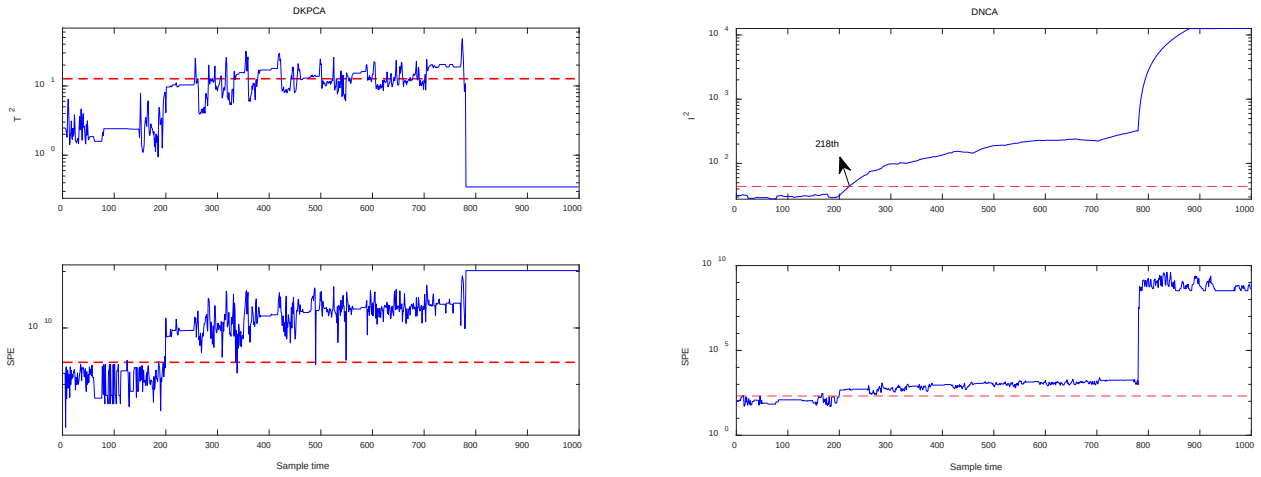

Fig. 11. HEV fault detection diagram of DKPCA and DNCA

From Fig. 11, it can be observed that due to their consideration of both the dynamic and nonlinear relationships of variables, both DKPCA and DNCA exhibit lower FARs, thus avoiding time and cost burdens for maintenance personnel. Additionally, both DKPCA and DNCA demonstrate excellent fault detection capabilities in terms of their *SPE* indices. In DKPCA, although most samples exceed the threshold for the T^2 index between the 200th and 800th samples, the value of the index starts to decrease significantly after the 800th sample. In contrast, the T^2 index of DNCA exceeds the threshold for the majority of samples. This helps maintenance personnel accurately determine whether faults have occurred, thereby preventing the deterioration of the HEV's reliability and performance. Although the fault begins to occur at the 200th sample and DNCA detects the fault at the 218th sample, its performance is still far superior to other methods.

In conclusion, the following conclusions can be drawn:

- Traditional dynamic methods such as DPCA fail to identify fault occurrences when highway third-level faults exhibit strong nonlinear characteristics due to their inability to consider the nonlinear relationships between variables. Using this method to monitor highway third-level faults will deteriorate the reliability and performance of the HEV.
- Traditional nonlinear methods such as KPCA overlook the dynamic relationships between variables, resulting in failure to accurately distinguish between normal data and faults. Even with the use of NCA to enhance nonlinear fitting capabilities, the monitoring effectiveness still requires further improvement. This is because NCA exhibits a longer detection delay and its *SPE* index has poor detection capabilities. Using these methods to monitor highway third-level faults will deteriorate the reliability and performance of the HEV.
- The proposed DNCA method not only inherits the outstanding nonlinear monitoring capabilities of NCA but also addresses dynamic monitoring issues. Compared to traditional methods, it exhibits shorter detection delays and stronger detection capabilities for its two indices, while also ensuring lower false alarm rates. This helps maintenance personnel to promptly identify fault occurrences, thereby preventing deterioration in the reliability and performance of HEV.

5 CONCLUSIONS

This paper investigates the process monitoring problem of high-speed three-level faults in HEVs. Due to the dynamic and nonlinear nature of these faults, we have chosen a novel dynamic nonlinear method --- DNCA. DNCA addresses the issue of neglecting variable autocorrelation relationships in the NCA method by integrating the time lag shift approach and proposing a method for determining the parameter q. The experimental results indicate that DNCA can more effectively monitor third-level highway faults with dynamic nonlinear characteristics. Firstly, we designed numerical simulation experiments: a dynamic nonlinear model was established, and three different types of faults were configured. The experimental results indicate that compared to traditional dynamic method DPCA, nonlinear methods such as KPCA and NCA, as well as dynamic nonlinear method DKPCA, DNCA not only has a lower FAR but also a higher FDR when dealing with dynamic nonlinear problems. Furthermore, we applied the DNCA method and traditional methods to real third-level highway fault data from HEV powertrain. The experimental results show that, compared to traditional methods, the DNCA method does not produce a high FAR before faults occur and can sensitively detect the onset of faults. This helps in promptly preventing deterioration in the reliability and performance of the HEV.

DNCA is a highly promising algorithm, and there are numerous avenues for future research:

- DNCA has not provided a quantitative method for determining parameters during iterative training using gradient descent, instead relying on previous experience. Further improvements can be made in the future.
- DNCA adopts the I^2 index from NCA, which introduces a detection delay issue, meaning it cannot respond promptly to the occurrence of faults. Further improvements can be made in the future.
- DNCA utilizes the time lag shift approach, which significantly increases the computational burden during offline training. Further improvements can be made in the future to enhance efficiency.

6 REFERENCES

[1] Chakraborty, R. and S. Das, Fault-Tolerant Technique against Current Sensors for Model Predictive Control of Induction Motor Drives. IEEE Transactions on Power Electronics, 2024.

[2] Hao, W., et al., KPI-related monitoring approach for powertrain system in hybrid electric vehicles. Energy Reports, 2024. 11: p. 3245-3255.

[3] Sepasiahooyi, S. and F. Abdollahi, Fault Detection of New and Aged Lithium-ion Battery Cells in Electric Vehicles. Green Energy and Intelligent Transportation, 2024: p. 100165.

[4] Veerendra, A.S., M.R.B. Mohamed, and F.P. García Márquez, Energy management control strategies for energy storage systems of hybrid electric vehicle: A review. Energy Storage, 2024. 6(1): p. e573.

[5] Zhang, Y., et al., Hierarchical eco-driving control strategy for connected automated fuel cell hybrid vehicles and scenario-/hardware-in-the loop validation. Energy, 2024: p. 130592.

[6] Yan, W., et al., Functional Analysis and Simulation Research on Powertrain of Hybrid Electric Vehicle. Automotive Digest, 2024(3).

[7] Yin, H., et al., A deep learning-based data-driven approach for predicting mining water inrush from coal seam floor using micro-seismic monitoring data. IEEE Transactions on Geoscience and Remote Sensing, 2023.

[8] Elmoazen, R., et al., Learning analytics in virtual laboratories: a systematic literature review of empirical research. Smart Learning Environments, 2023. 10(1): p. 23.

[9] Deng, W., et al., LSTMED: An uneven dynamic process monitoring method based on LSTM and Autoencoder neural network. Neural Networks, 2023. 158: p. 30-41.

[10] Zhao, X., Z. Wang, and G. Zheng, Knowledge-based integrated optimization design of agile imaging satellites' attitude controller and vibration isolator. Aerospace Science and Technology, 2023. 133: p. 108100.

[11] Ho, K.-F., P.-H. Chou, and M.-H. Chung, Comparison of nursing diagnostic accuracy when aided by Knowledge-Based Clinical Decision Support Systems with Clinical Diagnostic Validity and Bayesian Decision Models for psychiatric care plan formulation among nursing students: a quasi-experimental study. BMC nursing, 2023. 22(1): p. 142.

[12] Yan, W., et al., A review of real-time fault diagnosis methods for industrial smart manufacturing. Processes, 2023. 11(2): p. 369.

[13] Stoffel, P., et al., Evaluation of advanced control strategies for building energy systems. Energy and Buildings, 2023. 280: p. 112709.

[14] Bevans, B., et al., Monitoring and flaw detection during wire-based directed energy deposition using in-situ acoustic sensing and wavelet graph signal analysis. Materials & Design, 2023. 225: p. 111480.

[15] Bazrafshan, P., et al., A graph‐based method for quantifying crack patterns on reinforced concrete shear walls. Computer‐Aided Civil and Infrastructure Engineering, 2024. 39(4): p. 498-517.

[16] Zhou, X., et al., A new framework integrating reinforcement learning, a rule-based expert system, and decision tree analysis to improve building energy flexibility. Journal of Building Engineering, 2023. 71: p. 106536.

[17] Mondal, P.P., et al., Review on machine learning-based bioprocess optimization, monitoring, and control systems. Bioresource technology, 2023. 370: p. 128523.

[18] Xiao, B., et al., A fractal analytical model for Kozeny-Carman constant and permeability of roughened porous media composed of particles and converging-diverging capillaries. Powder Technology, 2023. 420: p. 118256.

[19] Xiao, X., et al., Analytical model for the nonlinear buckling responses of the confined polyhedral FGP-GPLs lining subjected to crown point loading. Engineering Structures, 2023. 282: p. 115780.

[20] Vettori, S., et al., An adaptive-noise Augmented Kalman Filter approach for input-state estimation in structural dynamics. Mechanical Systems and Signal Processing, 2023. 184: p. 109654.

[21] Veerakumar, N., et al., PMU-based real-time distribution system state estimation considering anomaly detection, discrimination and identification. International Journal of Electrical Power & Energy Systems, 2023. 148: p. 108916.

[22] Shadab, S., et al., Finite-time parameter estimation for an online monitoring of transformer: A system identification perspective. International Journal of Electrical Power & Energy Systems, 2023. 145: p. 108639.

[23] Diaz, M., P.-É. Charbonnel, and L. Chamoin, A new Kalman filter approach for structural parameter tracking: Application to the monitoring of damaging structures tested on shaking-tables. Mechanical Systems and Signal Processing, 2023. 182: p. 109529.

[24] Arsiwala, A., F. Elghaish, and M. Zoher, Digital twin with Machine learning for predictive monitoring of CO2 equivalent from existing buildings. Energy and Buildings, 2023. 284: p. 112851.

[25] Hao, W., et al., A Novel Dynamic Process Monitoring Algorithm: Dynamic Orthonormal Subspace Analysis. Processes, 2023. 11(7): p. 1935.

[26] Lou, Z., et al., Monitoring dynamic process with orthonormal subspace analysis. The Canadian Journal of Chemical Engineering, 2024.

[27] Lou, Z., et al., Thermal-Imaging-Based PCA Method for Monitoring Process Temperature. Processes, 2023. 11(2): p. 589.

[28] Wang, Y., et al., Survey on the theoretical research and engineering applications of multivariate statistics process monitoring algorithms: 2008–2017. The Canadian Journal of Chemical Engineering, 2018. 96(10): p. 2073-2085.

[29] Zhang, K., K. Zhang, and R. Bao, Prediction of gas explosion pressures: A machine learning algorithm based on KPCA and an optimized LSSVM. Journal of Loss Prevention in the Process Industries, 2023. 83: p. 105082.

[30] Li, X., et al., Source term inversion coupling Kernel Principal Component Analysis, Whale Optimization Algorithm, and Backpropagation Neural Networks (KPCA-WOA-BPNN) for complex dispersion scenarios. Progress in Nuclear Energy, 2024. 171: p. 105171.

[31] Lajmi, F., et al., Investigating machine learning and control theory approaches for process fault detection: a comparative study of KPCA and the observer-based method. Sensors, 2023. 23(15): p. 6899.

[32] Negiz, A., E. Lagergren, and A. Cinar. Statistical quality control of multivariable continuous processes. in Proceedings of 1994 American Control Conference-ACC'94. 1994. IEEE.

[33] Ku, W., R.H. Storer, and C. Georgakis, Disturbance detection and isolation by dynamic principal component analysis. Chemometrics and intelligent laboratory systems, 1995. 30(1): p. 179-196.

[34] Choi, S.W. and I.-B. Lee, Nonlinear dynamic process monitoring based on dynamic kernel PCA. Chemical engineering science, 2004. 59(24): p. 5897-5908.

[35] Attouri, K., et al., Improved fault detection based on kernel PCA for monitoring industrial applications. Journal of Process Control, 2024. 133: p. 103143.

[36] Lou, Z. and Y. Wang, New nonlinear approach for process monitoring: Neural component analysis. Industrial & Engineering Chemistry Research, 2020. 60(1): p. 387-398.

Paper submitted: 03.04.2024.
Paper accepted: 15.05.2024.